Ferromagnetism in the austenitic and martensitic states of Ni-Mn-In alloys

Thorsten Krenke, Mehmet Acet,* and Eberhard F. Wassermann
Fachbereich Physik, Experimentalphysik, Universität Duisburg-Essen, D-47048 Duisburg, Germany

Xavier Moya, Lluís Mañosa, and Antoni Planes
Facultat de Física, Departament d' Estructura i Constituents de la Matèria, Universitat de Barcelona, Diagonal 647, E-08028 Barcelona, Catalonia, Spain

(Received 30 May 2005; revised manuscript received 2 February 2006; published 15 May 2006)

The magnetic and structural transformations in the Heusler-based system $Ni_{0.50}Mn_{0.50-x}In_x$ are studied in the composition range $0.05 \leqslant x \leqslant 0.25$. While the cubic phase is preserved in the range $0.165 \leqslant x \leqslant 0.25$, we find the presence of martensitic transformations in alloys with $x \leqslant 0.16$. In a critical composition range $0.15 \leqslant x \leqslant 0.16$, the magnetic coupling in both austenitic and martensitic states is ferromagnetic. Magnetic field-induced structural transitions are also found in the $x=0.16$ alloy, whereby the structural transition temperature shifts by 42 K in a field of 50 kOe.

DOI: 10.1103/PhysRevB.73.174413 PACS number(s): 75.50.Cc, 81.30.Kf

I. INTRODUCTION

Heusler-based ferromagnetic (FM) Ni-Mn-Ga alloys with concentrations close to that of the stoichiometric compound Ni_2MnGa undergo martensitic transformations. In the martensitic state, the application of a magnetic field can cause strains up to about 10%.[1] This field-induced strain is known as the magnetic shape memory effect and is caused by the reorientation of martensite variants by twin boundary motion. The driving force for the reorientation is provided by the difference in the Zeeman energy of neighboring variants $\Delta \mathbf{M} \cdot \mathbf{H}$.[2] High saturation magnetization and high magneto-crystalline anisotropy are favorable for moving twin boundaries in low as possible external magnetic fields. In Ni-Mn-Ga alloys that transform martensitically, the magnetic ordering in both parent and product phases are FM, however with different exchange.[3]

With the aim of searching for other ferromagnetic Heusler alloys that transform martensitically, we have studied in a previous work the structural and magnetic properties of $Ni_{0.50}Mn_{0.50-x}Sn_x$ alloys.[4] Martensitic transformations were observed in alloys with concentrations up to 15 at % Sn. Similar results were also reported by Sutou *et al.*[5] In the narrow concentration range $0.13 \leqslant x \leqslant 0.15$, ferromagnetism and lattice instabilities were found to coexist, and an investigation of the magnetic properties had shown that the magnetic exchange in both parent and product phases are also FM as in Ni-Mn-Ga. However, in Ni-Mn-Sn, it was found that the magnetization of the low-temperature phase is smaller than that in the parent phase as opposed to the case in Ni-Mn-Ga alloys.[3]

For a systematic understanding of the properties of structural and magnetic transitions in Ni-Mn-based FM Heusler alloys, it is necessary to extend the studies to materials that incorporate other group IIIA-VA elements. In the present work, we examine the structural and magnetic properties of $Ni_{0.50}Mn_{0.50-x}In_x$ alloys by use of calorimetry, x-ray diffraction, optical microscopy, and magnetization.

II. EXPERIMENT

Ingots of about 3 g were prepared by arc melting the pure metals under argon atmosphere in a water-cooled Cu crucible and were remelted several times. The ingots were subsequently encapsulated under argon in quartz glass and annealed at 1073 K for 2 h. They were then quenched in ice water. The compositions of the alloys were determined by energy dispersive x-ray photoluminescence analysis (EDX) and are summarized in Table I. The corresponding valence electron concentration e/a is also given in the table. This is calculated as the concentration weighted sum of the number of $3d$ and $4s$ electrons of Ni and Mn and the number of $4s$ and $4p$ electrons of In. An estimated error of ±0.1% in determining the concentration leads to an error of ±0.007 in the value of e/a.

Polycrystalline samples of 30–100 mg cut from the ingots using a low-speed diamond saw were used as samples for magnetization and calorimetric studies. For the differential scanning calorimetry (DSC) measurements, one side of the samples was ground with 1200 grid SiC abrasive to insure proper thermal contact. Calorimetric measurements were carried out in the temperature range $120\ \mathrm{K} \leqslant T$

TABLE I. Compositions of the $Ni_{0.50}Mn_{0.50-x}In_x$ samples determined by EDX analysis and the valence electron concentrations per atom e/a.

x (nominal)	Ni	Mn	In	e/a
0.25	50.6	24.6	24.8	7.526
0.235	50.0	26.5	23.5	7.560
0.225	50.4	27.0	22.6	7.608
0.215	50.1	28.5	21.4	7.647
0.20	50.1	30.3	19.6	7.719
0.175	50.2	32.4	17.4	7.810
0.17	49.7	33.2	17.1	7.807
0.165	49.8	33.7	16.5	7.834
0.16	50.3	33.7	16.0	7.869
0.155	51.3	33.2	15.5	7.919
0.15	49.8	35.4	14.8	7.902
0.10	49.9	40.2	9.9	8.101
0.05	49.6	45.5	4.9	8.292

$\leqslant 830$ K in a DSC (TA Instruments MDSC 2920). For DSC measurements, the cooling and heating rates were 2–5 K/min. We have also used a second high sensitivity calorimeter for measurements in the temperature range 100 K$\leqslant T \leqslant$350 K. A third calorimeter was used for measurements under magnetic field.[6] The cooling rate in these measurements was 0.5 K/min.

The temperature dependence of the magnetization $M(T)$ in a low external magnetic field (H=50 Oe) was measured in the temperature range 5 K$\leqslant T \leqslant$380 K using a superconducting quantum interference device magnetometer. Prior to the measurements, the sample was prepared in a zero-field-cooled state (ZFC) by cooling it from 380 to 5 K in the absence of a magnetic field. Subsequently, the external field was applied and the data were taken on increasing temperature up to 380 K. Then, without removing the external field, the data were taken on decreasing temperature, i.e., field-cooled (FC). As a last step, again without removing the external field, the magnetization was measured on increasing temperature. The last step is denoted as the field-heated (FH) sequence. Any hysteresis in the FC and FH sequences is expected to be associated with a structural transition, whereas any splitting of the ZFC and FC curves below the FM transition temperatures is expected to be associated with pinning due to coexisting antiferromagnetic (AF) exchange, or pinning due to noncollinear magnetic structures that reside within twin boundaries if the system is martensitic. To further characterize the magnetic properties, the magnetic field dependence of the magnetization $M(H)$ was measured in fields up to 50 kOe.

Room-temperature structural analyses were carried out with conventional x-ray techniques using Cu $K\alpha$ radiation. The microstructure of the specimens was examined by optical microscopy. For this study, the samples with x=0.25 and 0.15 were polished and etched in Cr(IV) oxide solution with 5 V dc bias. For $x \leqslant 0.15$, nitric acid with 2% alcohol was used.

III. RESULTS

A. Calorimetric studies and identification of the transition temperatures

The results of calorimetric studies for the alloys with $0.16 \geqslant x \geqslant 0.05$ are plotted in Figs. 1(a)–1(e) in the temperature vicinity of the martensitic transformation. The heating and cooling cycles are indicated by arrows. For alloys with $x > 0.16$, no structural transformation is observed. On the other hand, alloys with $0.16 \geqslant x \geqslant 0.05$ exhibit a first-order structural transformation, for which the transition temperature increases with decreasing In concentration. We collect in Table II the characteristic transition temperatures at which martensite start and finish (M_s,M_f), and austenite start and finish (A_s,A_f) and the width of the hysteresis ΔT determined as the difference between the temperatures corresponding to the peak positions of the forward and reverse transitions. The superscripts *DSC* and *M* refer to the method used in determining the transition temperatures. For the alloys with $0.155 \geqslant x \geqslant 0.05$, the transition temperatures are taken as the

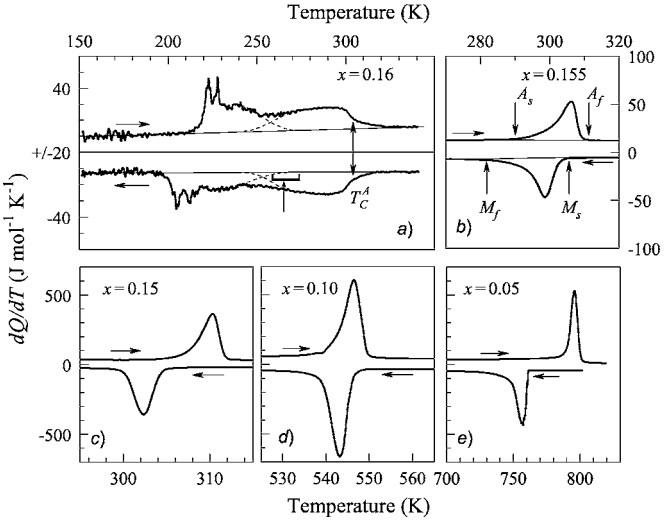

FIG. 1. dQ/dT vs temperature for the alloys undergoing martensitic transformations (a) x=0.16; (b) x=0.155; (c) x=0.15; (d) x=0.10; and (e) x=0.05. Horizontal arrows indicate direction of temperature change. The temperature region indicated by the bracket in part (a) is where the austenitic state begins to lose stability. Vertical arrows in part (b) exemplify the positions of the martensitic and austenitic transition temperatures.

temperatures where dQ/dT begin to deviate from the baselines. An example of the identification of the transition temperatures is shown in Fig. 1(b) with the vertical arrows. The transition temperatures determined in this manner from the calorimetry data are in very good agreement with those determined from the magnetization data (Sec. III C). The magnetization data allow only M_s and A_f to be identified.

The features in dQ/dT of the sample with x=0.16 seen in Fig. 1(a) are unlike those of the other samples. Here, the broad shoulder below the ferromagnetic Curie temperature of the austenitic state $T_C^A \approx 300$ K (Sec. III C 2) overlaps with the features of the first-order structural transformation. This makes it difficult to determine the exact positions of M_s and A_f, whereas M_f and A_s can be identified. Also, the presence of multiple peaks observed in dQ/dT both in the forward and reverse transitions, especially the double-peak structure with nearly identical separations in the heating and cooling curves, suggests that intermartensitic transitions could be occurring. The observed data can be understood to be due to the superposition of the contributions from the features associated with the magnetic and structural transitions. The dashed lines are guides representing the overlapped contributions, and it would be expected that M_s lies within the temperature range of the bracket shown in the figure. This range falls within ±10 K of M_s^M, the martensite start temperature determined from the magnetization data (Sec. III C 2).

The entropy and enthalpy changes (ΔS and ΔH, respectively) around the structural transitions are calculated from the baseline-corrected calorimetry data.[4] The values of ΔH and ΔS, determined as the average obtained from the cooling and heating experiments, are also included in Table II.

As will become evident from the magnetization data presented in Sec. III C, the sample with x=0.16 exhibits a mag-

TABLE II. Martensite start and finish temperatures (M_s,M_f), austenite start and finish temperatures (A_s,A_f) determined by DSC and $M(T)$ measurements (*DSC* and *M* in superscript) and the enthalpy and entropy changes (ΔH,ΔS) around the transition.

x	M_s^{DSC} (K)	M_s^{M} (K)	M_f^{DSC} (K)	A_s^{DSC} (K)	A_f^{DSC} (K)	A_f^{M} (K)	ΔT (K)	ΔH (J mol^{-1})	ΔS (J mol^{-1} K^{-1})
0.16		264	195	208		266		204±17	0.92±0.03
0.155	305	306	282	290	311	311	8	296±0.1	0.98±0.01
0.15	305	309	299	304	312	315	8	927±20	3.03±0.13
0.10	549		532	534	551		3	2814±157	5.15±0.31
0.05	760		720	782	803		40	3529±359	4.55±0.48

netic field-induced transformation. Therefore, we have studied dQ/dt vs T for this sample under various constant magnetic fields. The measurements were done on cooling only. The results plotted in Fig. 2 show the data in the full temperature range of the measurements and in the temperature region of the major feature around the martensitic transition (inset). The rate of shift in the position of the major peak (and thereby the position of M_s) with respect to field amounts to -0.8 K kOe^{-1} (-8 K T^{-1}). This value is also found in temperature-dependent magnetization measurements measured in 50 kOe presented at the end of this paper.

B. Structural properties

Figure 3 shows x-ray diffraction patterns taken at room temperature for the alloys with $x=0.25$ and $x=0.16$. For $x=0.25$, superstructure reflections of the $L2_1$ phase ($Fm3m$) are also observed. By replacing In with Mn, the lattice constants of the austenitic phase become smaller, and the peak positions shift to larger angles. The superstructure reflections are not present for $x=0.16$. The crystal structure in this case is $B2$ ($Pm3m$), for which the lattice constants are half as large as that of the $L2_1$ phase.

The alloys with $x \leqslant 15.5$ are martensitic at room temperature in agreement with the calorimetric measurements. The samples with $x=0.155$ and $x=0.15$ have a 10 M modulated martensite structure. Figure 4 shows the diffraction pattern with the inset showing the details in the range $40° \leqslant 2\theta \leqslant 44.5°$. The unit cells are monoclinic with $\beta=88.45°$ and 88.93° for $x=0.155$ and $x=0.15$, respectively.

The diffraction pattern of the alloy with $x=0.10$ (Fig. 5) is related to that of a 14 M martensitic structure. The inset shows the details in the range $40° \leqslant 2\theta \leqslant 46.5°$. The unit cell here is also monoclinic with $\beta=93.67°$. For $x=0.05$, the martensite has an unmodulated tetragonal $L1_0$ structure as seen in Fig. 6.

Such structures are also observed in Ni-Mn-Ga, Ni-Mn-Al, and Ni-Mn-Sn alloys.[4,7–9] The crystal structures and the lattice constants obtained from x-ray diffraction experiments are collected in Table III.

The room-temperature microstructure of the alloys is shown in Figs. 7(a)–7(e). These show optical microscopy images of the surface of the alloys with $x=0.05$, 0.10, 0.15, 0.155, and 0.25. Figure 7(a) shows the surface of the sample with $x=0.25$, for which the grain size varies between 50 and 300 μm. The black spots are voids caused by the etch process during surface preparation.

Figures 7(b)–7(e) show the microstructure of the samples that are martensitic at room temperature. No phase separation can be identified, in agreement with the x-ray diffraction patterns. The grain size in all images lies within 50–300 μm. Although the crystal structures are different, the morphologies of the 10*M*, 14*M*, and the unmodulated

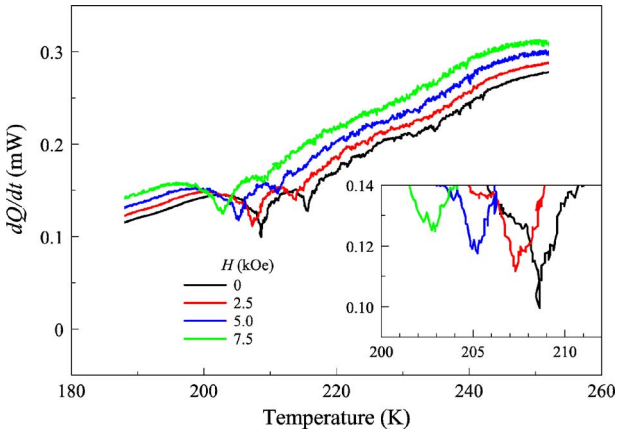

FIG. 2. (Color online) dQ/dt vs T taken on cooling and under various magnetic fields. The inset shows the data in the temperature region of the major feature around the martensitic transition. The rate of shift in M_s with respect to field amounts to -0.8 K kOe^{-1}.

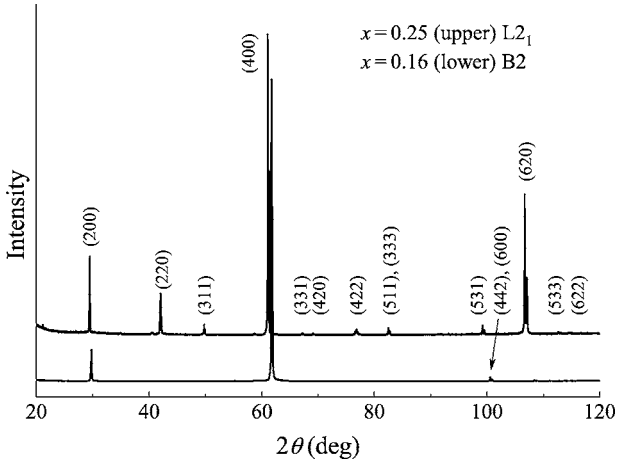

FIG. 3. X-ray diffraction pattern at room temperature for $x=0.25$ (upper) and $x=0.16$ (lower). The crystal structure is $L2_1$ for $x=0.25$ and $B2$ for $x=0.16$.

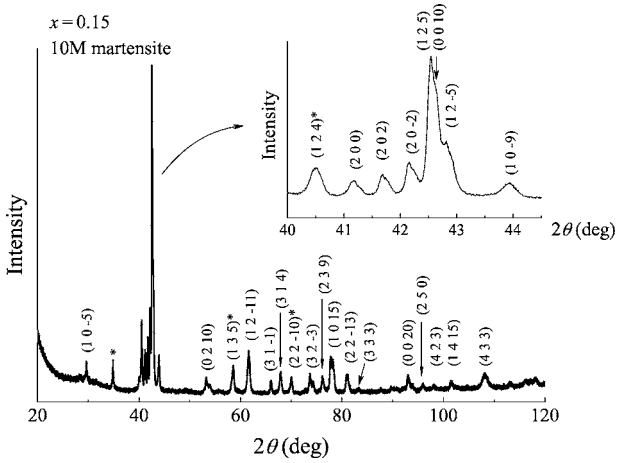

FIG. 4. X-ray diffraction pattern at room temperature for $x=0.15$. The inset shows details in the range $40° \leqslant 2\theta \leqslant 44.5°$. The crystal structure is $10M$ with a monoclinic unit cell.

phases are similar. In all three cases, the martensite is plate-like, which can be recognized by the linear grain boundary of each plate.

C. Magnetic properties

1. Samples with compositions $0.25 \geqslant x \geqslant 0.165$

Figure 8(a) shows $M(T)$ for the sample with $x=0.20$ and $x=0.25$. The behavior of $M(T)$ for $x=0.25$ is that of a typical ferromagnet. The Curie temperature T_C is 290 K, and even in a low external magnetic field of 50 Oe, the FC curve retraces the ZFC curve at a magnetization value corresponding to the demagnetizing limit of the sample, indicating no structural transitions. The FH curve also retraces the FC and ZFC curves. $M(H)$ data at various temperatures are given in Fig. 8(b). The magnetization saturates at low temperatures, and at 290 K (T_C) the saturation weakens, leading to a finite high-field susceptibility. $M(H)$ at 350 K, which corresponds to the paramagnetic state, shows linear behavior.

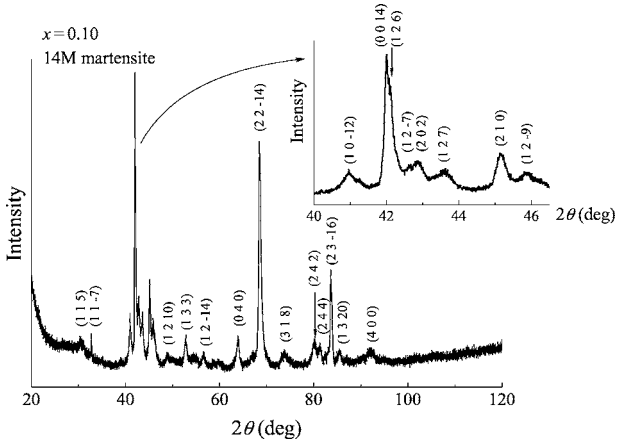

FIG. 5. X-ray diffraction pattern at room temperature for $x=0.10$. The inset shows details in the range $40° \leqslant 2\theta \leqslant 46.5°$. The crystal structure is $14M$ with a monoclinic unit cell.

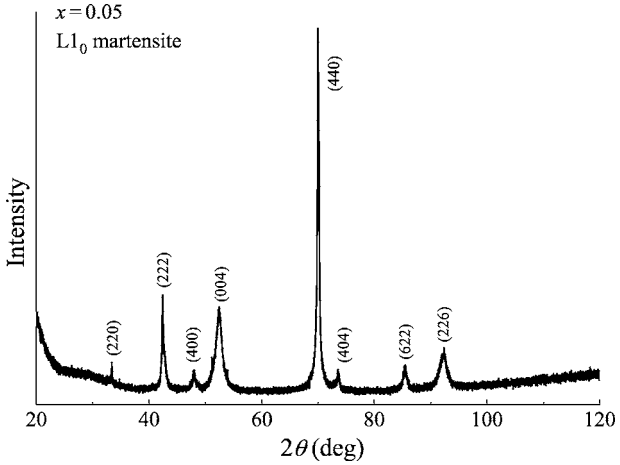

FIG. 6. X-ray diffraction pattern at room temperature for $x=0.05$. The crystal structure is $L1_0$.

As Mn is substituted for In, excess Mn atoms occupy In sites. In such spatial configurations, Mn-Mn neighbors have a smaller separation than that in the stoichiometric compound. This can introduce AF exchange, which can pin the FM domains in various configurations depending on whether the sample is cooled through T_C in a small ($H \approx 50$ Oe) external field or not.[10,11] This causes a separation of the FC and ZFC curves, which is seen in the $M(T)$ data of the samples with $x=0.20$ and $x=0.17$ in Figs. 8(a) and 9(a), respectively. However, contrary to what is expected, the splitting weakens with decreasing In concentration, from $x=0.20$ to $x=0.17$, and at $x=0.165$, the splitting vanishes [Fig. 9(b)]. There is also a marginal increase in T_C from 290 K for $x=0.25$ to 310 K for $x=0.165$, indicating a strengthening of the FM exchange interaction.

In Fig. 10(a), $M(H)$ at 5 K measured on samples with $0.25 \geqslant x \geqslant 0.165$ are compared. All data show saturation

TABLE III. Crystal structures and lattice parameters of $Ni_{0.50}Mn_{0.50-x}In_x$ at room temperature. The structures of the samples with $x=0.155$, $x=0.15$, and $x=0.10$ are monoclinic with $\beta=88.45°$, 88.93°, and 93.67°, respectively.

	Crystal	Lattice parameter		
x	structure	a(Å)	b(Å)	c(Å)
0.25	$L2_1$	6.071	6.071	6.071
0.235	$L2_1$	6.060	6.060	6.060
0.225	$L2_1$	6.055	6.055	6.055
0.215	$L2_1$	6.043	6.043	6.043
0.20	$L2_1$	6.031	6.031	6.031
0.175	$L2_1$	6.018	6.018	6.018
0.17	$L2_1$	6.018	6.018	6.018
0.165	$L2_1$	6.004	6.004	6.004
0.16	$B2$	3.004	3.004	3.004
0.155	$10M$	4.385	5.592	21.190
0.15	$10M$	4.391	5.882	21.184
0.10	$14M$	4.284	5.811	30.109
0.05	$L1_0$	7.593	7.593	6.980

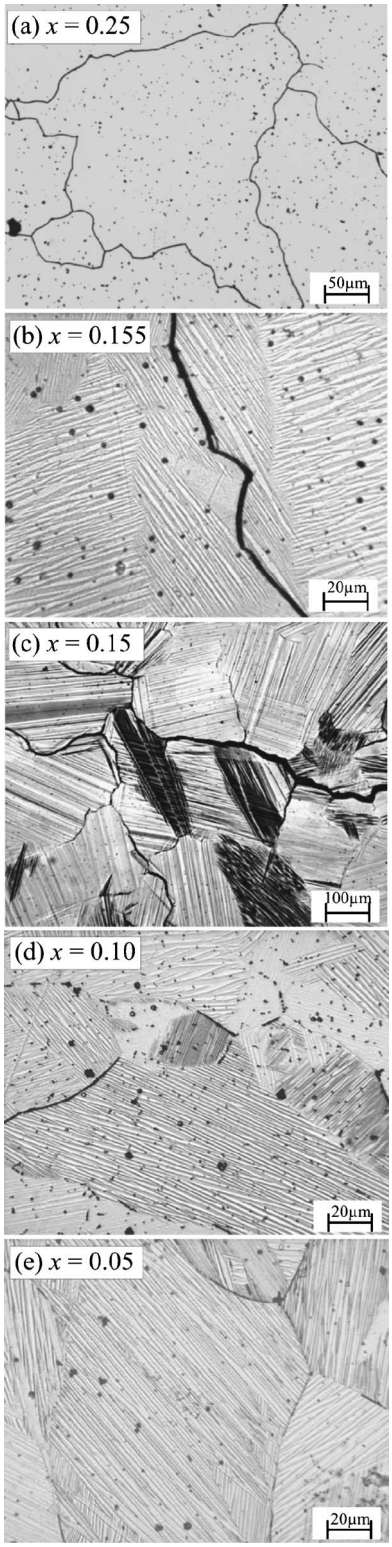

FIG. 7. Optical microscopy images of the microstructure for $x=0.25$, $x=0.155$, $x=0.15$, $x=0.10$, and $x=0.05$.

above 15 kOe. Furthermore, the saturation magnetization increases with decreasing In concentration from about 80 emu g^{-1} ($x=0.25$) to about 119 emu g^{-1} ($x=0.165$). The increase is effectively linear in concentration as seen for the saturation magnetization per formula unit σ_s plotted in Fig. 10(b). However, if it is assumed that Ni and In carry essentially no moment, the moment on the Mn atom remains constant throughout the studied concentration range. Generally, one would expect σ_s to decrease as Mn-Mn neighbors appear with decreasing In concentration, as in the case of other Ni-Mn-based Heusler alloys. We discuss this point in Sec. IV.

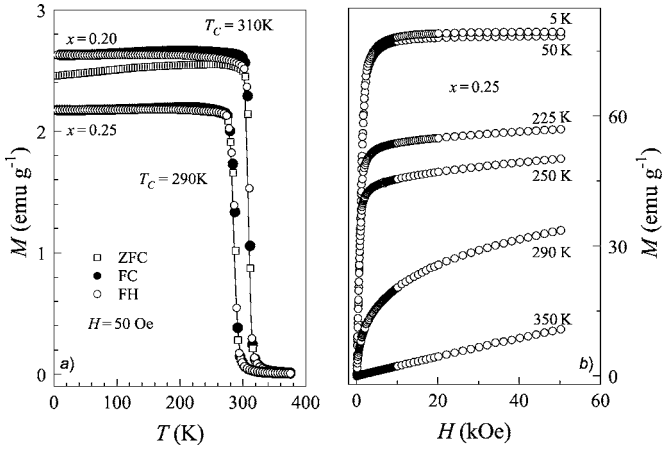

FIG. 8. (a) ZFC, FC, and FH $M(T)$ of the samples with $x=0.25$ and $x=0.20$ in $H=50$ Oe and (b) $M(H)$ of the sample with $x=0.25$. Prior to each $M(H)$ measurement, the samples were prepared in the ZFC state by bringing them above 380 K.

2. *Samples with compositions* $0.16 \geqslant x \geqslant 0.15$*: Identification of transition temperatures in* $M(T)$

As the In concentration is further decreased, we reach the situation shown in Fig. 11(a), where $M(T)$ is plotted for the sample with $x=0.16$. The FH data do not retrace the FC data but show a hysteresis [Fig. 11(b)], indicating a first-order structural transition as found in the results of the calorimetric measurements.

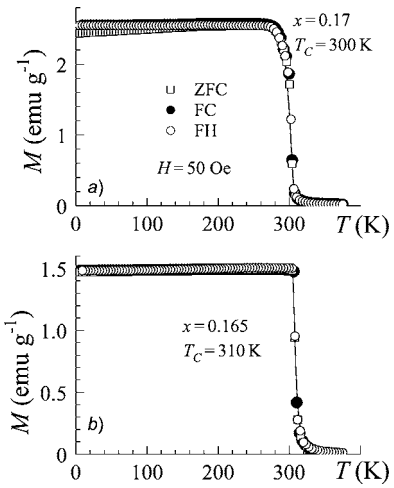

FIG. 9. ZFC, FC, and FH $M(T)$ in $H=50$ Oe of the samples with (a) $x=0.17$ and (b) $x=0.165$. Prior to each $M(H)$ measurement, the samples were prepared in the ZFC state by bringing them above 380 K.

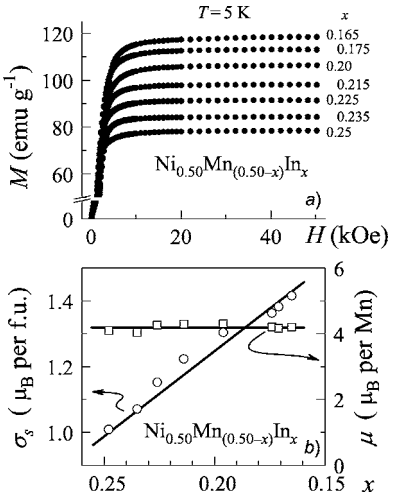

FIG. 10. (a) $M(H)$ at 5 K of samples with $0.165 \leqslant x \leqslant 0.25$. (b) The magnetic moment per formula unit and the magnetic moment on Mn determined by assuming no moment on Ni and In for the samples with $0.165 \leqslant x \leqslant 0.25$.

At high temperatures, in the austenitic state, the sample is paramagnetic and orders ferromagnetically below $T_C^A = 300$ K. However, as the temperature decreases, instead of $M(T)$ running at a constant value, as expected from a ferromagnet, it begins to decrease after reaching a maximum. Below this point the austenitic state begins to lose stability. Therefore, the temperature corresponding to this maximum is taken as M_s. Its value of 264 K corresponds approximately to the temperature at which the feature associated with the structural transition in the cooling DSC curve approaches the base line [vertical arrow in Fig. 1(a)]. Similarly, in the reverse transformation, A_f is identified as the maximum in $M(T)$ lying at about 275 K. Below M_s, $M(T)$ decreases with decreasing temperature and reaches a minimum as the proportion of FM austenite progressively decreases. Since the martensitic state is not ferromagnetic in this temperature regime (ferromagnetism appears below T_C^M), the total magnetization of the mixed austenite-martensite decreases. Namely, the martensite acts as a nonferromagnetic entity lowering the total magnetization. As the sample is further cooled, a second FM transition occurs at $T_C^M \approx 200$ K, which lies close to M_f determined from the DSC measurements. Below T_C^M, a large separation between FC and ZFC curves [Figs. 11(a) and 11(b)] is found. Due to the reduced symmetry of the martensitic state with respect to the cubic austenitic state, the number of easy axes can decrease, which in turn can be accompanied by an increase in the magnetic anisotropy. The increase in anisotropy can be seen in the low-field region of $M(H)$ shown in detail in Fig. 11(d), where the initial slope of the magnetization decreases with decreasing temperature. Under these circumstances, the magnetic domain configuration below T_C^M will depend on the external cooling field conditions as the sample is cooled through T_C^M. This leads to the observed splitting in the FC and ZFC curves. A similar effect has also been observed in the Ni-Mn-Ga system.[12]

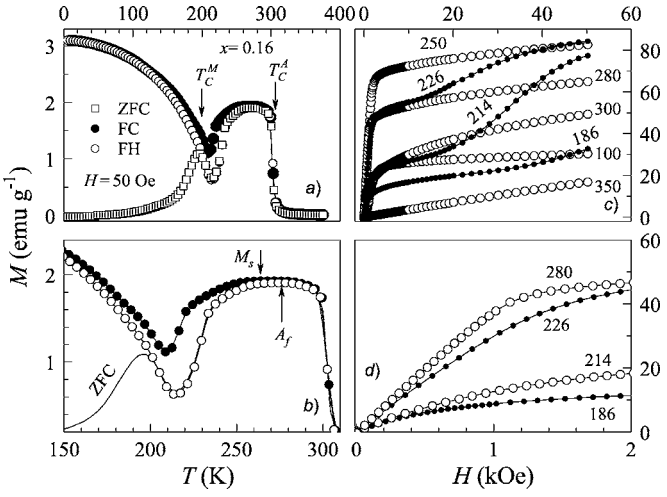

FIG. 11. (a) ZFC, FC, and FH $M(T)$ of the sample with $x=0.16$ in $H=50$ Oe. (b) $M(T)$ plotted in a temperature range around the martensitic transition. (c) $M(H)$ at selected temperatures given at the right of the figures in kelvin. Prior to each $M(H)$ measurement, the samples were prepared in the ZFC state by bringing them above 380 K. (d) $M(H)$ shown for the low-field region. The slope of the initial magnetization decreases with increasing temperature as the magnetic anisotropy strengthens.

$M(H)$ for $x=0.16$ is plotted in Fig. 11(c) at various temperatures. Here, it is seen that $M(H)$ does not saturate at temperatures in the range $M_s \leqslant T \leqslant T_C^A$, indicating that even at these temperatures within the austenitic phase, the FM state incorporates nonferromagnetic entities. The $M(H)$ data shown with closed symbols at 186, 214, and 226 K in Fig. 11(c) indicate the presence of a field-induced transition, whereby at 50 kOe, $M(H)$ at 214 and 226 K approach values similar to those of $M(H)$ at 250 K. Although 186 K is lower than M_f determined from DSC measurements, an upturn in the curve associated with the field-induced transition is also found in $M(H)$ at about 40 kOe.

$M(T)$ and $M(H)$ for $x=0.155$ are shown in Fig. 12. Around room temperature the sample undergoes a martensitic transformation, whereby the positions of the maxima in the FC and ZFC $M(T)$ curves correspond to M_s and A_f respectively [Fig. 12(b)]. Other than this, there is a second feature in $M(T)$ about 20 K below M_s indicated as T^*. To understand the nature of this feature, it is necessary to examine $M(H)$ [Fig. 12(c)] at various temperatures and $M(T)$ in 50 kOe [Fig. 12(d)]. $M(H)$ at 330 and 290 K, i.e. on both sides and in the vicinity of M_s, show linear behavior. However, the data at 330 K reach higher values than those at 290 K at the same field values. Namely, the magnetic short-range correlations in the paramagnetic $L2_1$ state at 330 K are stronger than those at 290 K, which is below M_s. Indeed, considering the high-temperature end of the curve in Fig. 12(d), $M(T)$ increases with decreasing temperature in a manner that would approach an austenitic Curie temperature T_C^A as shown by the dashed guideline. However, before T_C^A can be reached, the structural transformation takes place at M_s—the value of which is not altered in 50 kOe. $M(T)$ data show that hysteresis between FC and FH $M(T)$ curves prevails at temperatures around T^*, and persists to temperatures down to below 70 K. This suggests that the martensitic transition is not complete and austenite coexists in the sys-

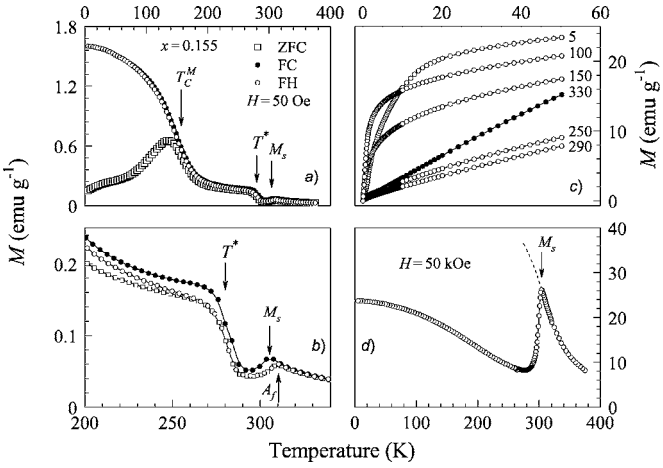

FIG. 12. (a) ZFC, FC, and FH $M(T)$ of the sample with $x=0.155$ in $H=50$ Oe. (b) $M(T)$ plotted in a temperature range around the martensitic transition. (c) $M(H)$ at selected temperatures given at the right of the figures in kelvin. Closed symbols pertain to data for $T>M_s$. Prior to each $M(H)$ measurement, the samples were taken above 380 K and prepared in the ZFC state. (d) $M(T)$ in 50 kOe.

tem. Therefore, the feature at T^* can be closely related to T_C^A, below which remaining austenite orders ferromagnetically. The ZFC and FC magnetization curves separate below $T_C^M \approx 135$ K [Fig. 12(a)] for similar reasons discussed for the case of the $x=0.16$ alloy. The form of the $M(H)$ curves below and above T_C^M is also an indication of ferromagnetic ordering in the martensitic state.

With regard to T^*, a similar situation occurs for the alloy with $x=0.15$, which we discuss next.

$M(T)$ and $M(H)$ for $x=0.15$ are plotted in Fig. 13. The features in the data are similar to those for the data of the $x=0.155$ alloy, but $M(T)$ in 50 Oe is about 2 orders of magnitude smaller. Here also, the values of M_s and A_f are in good agreement with those obtained from the DSC measurements. $M(H)$ at temperatures above and below M_s have similar character with those for the $x=0.155$ alloy, i.e., the magnetic correlations in the austenitic state are stronger than those in the martensitic state. The tendency of the austenitic state to order magnetically is also observed in $M(T)$ for this sample. However, the sample transforms martensitically before magnetic ordering can occur. Similar to the situation for $x=0.155$, there is hysteresis between the FC and FH $M(T)$, showing that austenite is present in the sample. Here also, the position of T^* could be related to T_C^A.

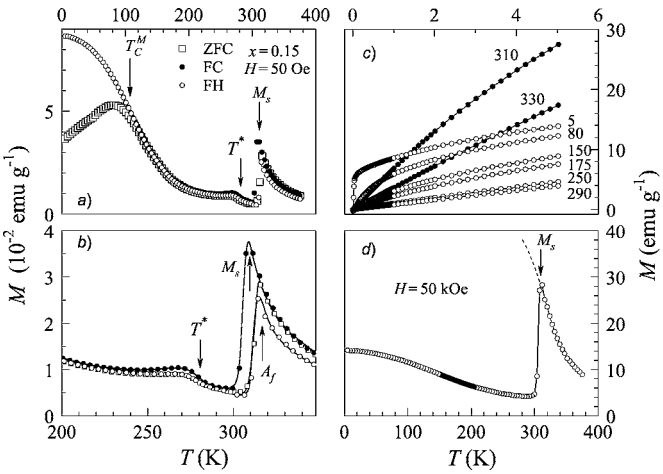

FIG. 13. (a) ZFC, FC, and FH $M(T)$ of the sample with $x=0.15$ in $H=50$ Oe. (b) $M(T)$ plotted in a temperature range around the martensitic transition. (c) $M(H)$ at selected temperatures given at the right of the figures in kelvin. Closed symbols pertain to data for $T>M_s$. Prior to each $M(H)$ measurement, the samples were prepared in the ZFC state by bringing them above 380 K. (d) $M(T)$ in 50 kOe.

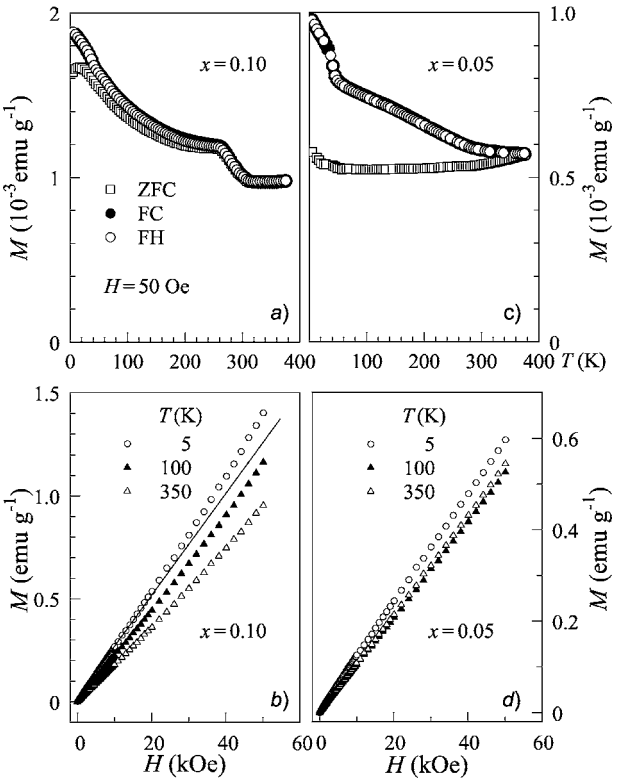

FIG. 14. (a) ZFC, FC, and FH $M(T)$ for $x=0.10$ and (b) $M(H)$ at 5, 100, and 350 K. (c) ZFC, FC, and FH $M(T)$ for $x=0.05$ and (d) $M(H)$ at 5, 100, and 350 K.

3. *Samples with compositions* $x=0.10$ *and* $x=0.05$

At lower In concentrations, long-range FM ordering no longer occurs. This can be seen in the $M(T)$ and $M(H)$ data for the samples with $x=0.10$ and $x=0.05$ in Fig. 14. These samples transform martensitically above room temperature. The magnetization of these samples are about 3 orders of magnitude smaller in 50 Oe than in the case for the samples with well-defined FM ground states. For $x=0.10$, $M(H)$ seen in Fig. 14(b) is essentially linear at 350 K, but at 100 and 5 K an upward curvature is observed with respect to the linear reference line drawn in the figure. Such behavior can be attributed to the gradual reorientation of noncollinear spins in the direction of the magnetic field. For $x=0.05$, $M(H)$ is linear at all temperatures, whereby it can be expected that the interactions become AF at this concentration

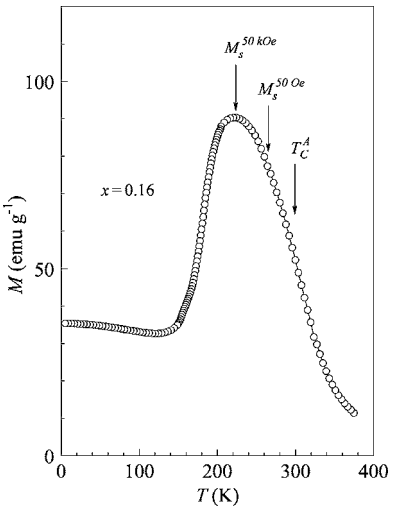

FIG. 15. $M(T)$ measured in 50 kOe for $x=0.16$. M_s is lowered by about 40 K in 50 kOe.

as the composition of the antiferromagnet $Ni_{0.50}Mn_{0.50}$ is approached.

IV. DISCUSSION

The Ni-Mn-In system near the Heusler composition shows marked differences in the magnetic properties from those of other Ni-Mn-based Heusler alloys. The major feature that particularly stands out is the increase of σ_s with increasing Mn concentration. As for other Ni-Mn-based Heuslers, one would expect a weakening of the magnetic moment with increasing Mn concentration due to the decreased distance of the Mn-Mn bonds, thus leading to AF exchange. It appears that the considerably larger size of the In atom as compared to other group IIIA and group IVA elements (other than *T*l) leads to a Mn-Mn separation that is large enough so that AF exchange of substantial strength cannot develop. In Ni-Mn-Sn and Ni-Mn-Ga Heusler alloys, where Sn has a smaller atomic radius than In, and the lattice constants of the alloys are smaller than in Ni-Mn-In at similar compositions, AF interactions do appear with increasing Mn content.[4,20] Any weak AF exchange that develops in $Ni_{0.50}Mn_{0.50-x}In_x$, as evident in the separation of ZFC and FC curves for the alloys with compositions $0.25 \geqslant x \geqslant 0.165$, is essentially suppressed by the magnetization of the ferromagnetic matrix in high magnetic fields, so that $M(H)$ reaches saturation [Fig. 10(a)]. This property is found in the alloys that do not undergo a martensitic transformation. However, to understand the exact cause of the increase of σ_s with increasing Mn concentration, the band structure giving the details of the overlap of p and d states is required. This would also explain why the ZFC-FC splitting weakens with increasing Mn concentration in the range $0.20 \geqslant x \geqslant 0.17$ and vanishes for $x=0.165$.

In the case of the alloys that undergo martensitic transformations, one observes that high external fields do not wash out the features around the martensitic transitions as observed in Figs. 12 and 13. Instead, the features are accentuated. This is also the case for the alloy with $x=0.16$, for which $M(T)$ in 50 kOe is shown in Fig. 15. However, unlike the other two samples with $x=0.155$ and $x=0.15$ that transform martensitically and show no shift in the transition temperatures, this alloy shows a strong shift of about 40 K in M_s on applying a field of 50 kOe amounting to a rate of change of M_s with respect to field of -0.8 K kOe^{-1}. This value is the same as that found in the calorimetric measurements in field (Fig. 2). M_s in 50 kOe ($M_s^{50\ kOe}=225$) K and 50 Oe ($M_s^{50\ Oe}=264$) K are shown in the figure. These data, along with the calorimetric data, indicate that the upturn in the $M(H)$ curves observed in the data of Fig. 11(c) is attributed to a field-induced transition from the martensitic to the austenitic state. This situation is opposite to what is observed for Ni-Mn-Ga alloys, where an external field causes M_s to shift to higher values.[13]

For alloys that undergo martensitic transformations around and below room temperature, a good agreement can be reached in the transition temperatures determined by $M(T)$ measurements in small magnetic fields and DSC measurements. The agreement is observed in the values of M_s and A_f for $x=0.155$ and $x=0.15$ collected in Table II and corresponds to the onset of the deviation from "normal" ferromagnetic behavior in $M(T)$ and the onset of the deviation from the baseline in dQ/dT. However, in the latter case, the uncertainty in the positioning of the baseline can make a difference in determining M_s^{DSC}. On the other hand, determining the position where $M(T)$ deviates from normal behavior requires no reference and is easily observed if considerable difference in strength of magnetic exchange accompanies the structural transition. Once M_s^M has been determined, M_s^{DSC} can be self-consistently cross checked, and the DSC results for the alloys with lower In concentrations ($x=0.10$ and 0.05) can then be used to estimate their martensitic transition temperatures.

On the other hand, determining and cross checking M_f and A_s is not as straightforward. The prevalence of the hysteresis observed in FC and FH $M(T)$ down to low temperatures suggests that the austenitic phase is still present in a broad temperature range, whereas DSC measurements cannot resolve the presence of an austenitic state at the same temperatures. For practical purposes, however, M_f and A_s are estimated from the DSC measurements as described in the preceding paragraph. Neutron diffraction studies are required to confirm that the hysteresis in $M(T)$ is linked to the presence of austenite at low temperatures.

The high-field $M(T)$ results, together with the DSC, and low-field magnetization studies show that $x=0.16$ is a critical concentration that separates alloys that transform martensitically from those that are stable in the $L2_1$ or the $B2$ phase. It is also the only composition that exhibits a field-induced transition. For a better understanding of the magnetic and structural changes occurring around the martensitic transition, magnetic field-dependent neutron diffraction experiments and magnetic field-dependent calorimetric measurements on the alloys with concentrations in the critical region are required.

Figure 16 shows the structural and magnetic transition temperatures as a function of the valence electron concentration. This diagram resembles that of the Ni-Mn-Sn system. [4] Whereas T_C^M shows very little change with e/a, the change in

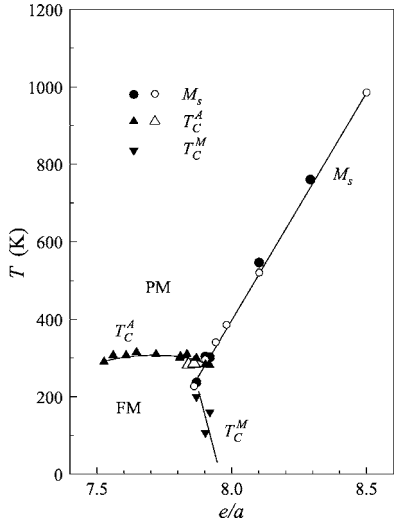

FIG. 16. The structural and magnetic transition temperatures as a function of the valence electron concentration for Ni-Mn-In. The open symbols represent values obtained from literature (Refs. 5 and 14).

T_C^M is relatively rapid. The temperatures corresponding to T^* of the $x=0.155$ and $x=0.15$ alloys are also included as T_C^A data in the diagram. M_s, on the other hand, decreases with deceasing e/a and is expected to vanish around $x=0.17$. In the critical composition range $0.16 \geqslant x \geqslant 0.15$, which corresponds to about $7.92 \geqslant e/a \geqslant 7.87$, the martensitic phase is FM at low temperatures.

The e/a dependence of the M_s temperatures of Ni-Mn-based Heusler systems is plotted in Fig. 17. The data are from the present study and earlier work.[4,5,15–17] Instead of the data following a single curve, which would have supported e/a to have a universal character for the Heusler alloys, [18,19,21] they have different slopes originating from their common point corresponding to $Ni_{0.50}Mn_{0.50}$ ($e/a=8.5$). Therefore, a simple choice of e/a as the concentration weighted valence electron per atom can only be considered to be a guideline for examining systematic changes only within a single-alloy system. A study on isoelectronic alloys obtained by substituting In for Ga to obtain Ni-Mn-Ga-In shows that, although e/a remains unchanged, the structural and magnetic transition temperatures vary considerably.[22]

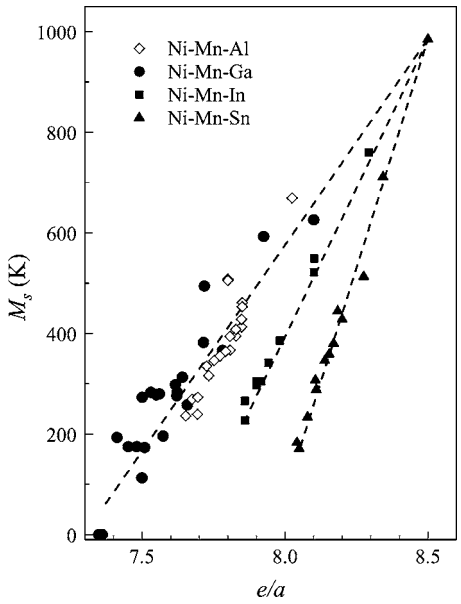

FIG. 17. Martensitic start temperatures of the studied manganese-based Heusler systems Ni-Mn-Ga, Ni-Mn-Al, Ni-Mn-Sn, and Ni-Mn-In.

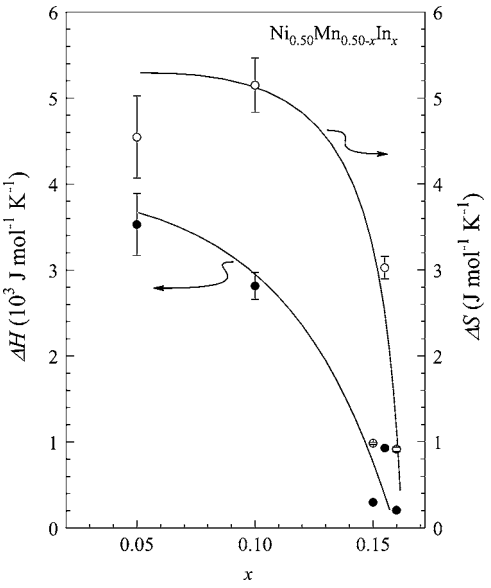

FIG. 18. ΔS and ΔH as a function of e/a.

The entropy and enthalpy changes at the martensitic transition calculated from the heat flow data are plotted in Fig. 18. Both ΔS and ΔH decrease with increasing In concentration. For systems where the main contribution to ΔS is vibrational, such as in Cu-based Heusler alloys, there is no significant concentration dependence.[23] On the other hand, a similar concentration dependence has been reported for Ni-Mn-Sn alloys, where the difference in the magnetic exchange interactions below and above M_s is large.[4] In fact, this large difference gave rise to a positive magnetic entropy change in the vicinity of the martensitic transformation leading to a large inverse magnetocaloric effect.[24] A similar effect can also be expected to occur in the Ni-Mn-In system.

For a magnetic shape memory effect to occur at all, the presence of ferromagnetism in the martensitic state is necessary. The alloy with $x=0.16$ is a particularly interesting candidate, since M_s lies around room temperature and the alloy becomes FM at a lower temperature. The present study will also be complemented by magnetic field-induced strain studies to address the question as to whether a magnetic shape memory effect occurs in these alloys.

V. CONCLUSION

The type of modulated structure of martensite in $Ni_{0.50}Mn_{0.50-x}In_x$ is found by x-ray studies to depend on the In composition. The structure changes in a $10M$, $14M$, and $L1_0$ sequence as the In concentration decreases.

In a critical composition range $0.15 \leqslant x \leqslant 0.16$, the austenitic and martensitic phases are FM. However, the ferromagnetism of the parent and product phases is characterized by separate magnetic transition temperatures. The low-temperature phase incorporates ferromagnetic components with complex magnetic domain structures which are coupled to the lattice degree of freedom. This is suggested by the splitting of the ZFC and FC curves measured in low external magnetic fields. For $x=0.16$ a magnetic field-induced transitions at temperatures $T<M_s$ are observed. The strong shift in M_s^M suggests that the induced transition is structural. Due to the induced structural transition, the $x=0.16$ sample is likely to exhibit large field-induced strains. We furthermore find that the features found in the low external magnetic field $M(T)$ data, especially the rapid decrease of the magnetization below M_s, are retained when the measurements are performed in high magnetic fields.

ACKNOWLEDGMENTS

We thank Peter Hinkel and Sabine Schremmer for technical support. This work was supported by Deutsche Forschungsgemeinschaft (GK277) and CICyT (Spain), Project MAT2004-1291. X.M. acknowledges support from DGICyT (Spain).

*Electronic address: macet@ttphysik.uni-duisburg.de

[1] A. Sozinov, A. A. Likhachev, N. Lanska, and K. Ullakko, Appl. Phys. Lett. **80**, 1746 (2002).
[2] R. C. O'Handley, J. Appl. Phys. **83**, 3263 (1998).
[3] R. Tickle and R. D. James, J. Magn. Magn. Mater. **195**, 627 (1999).
[4] T. Krenke, M. Acet, E. F. Wassermann, X. Moya, L. Mañosa, and A. Planes, Phys. Rev. B **72**, 014412 (2005).
[5] Y. Sutou, Y. Imano, N. Koeda, T. Omori, R. Kainuma, K. Ishida, and K. Oikawa, Appl. Phys. Lett. **85**, 4358 (2004).
[6] J. Marcos, F. Casanova, X. Batlle, A. Labarta, A. Planes, and L. Mañosa, Rev. Sci. Instrum. **74**, 4768 (2003).
[7] R. Kainuma, H. Nakano, and K. Ishida, Metall. Mater. Trans. A **27**, 4153 (1996).
[8] J. Pons, V. A. Chernenko, R. Santamarta, and E. Cesari, Acta Mater. **48**, 3027 (2000).
[9] C. Jiang, Y. Muhammad, L. Deng, W. Wu, and H. Xu, Acta Mater. **52**, 2779 (2004).
[10] E. Duman, M. Acet, Y. Elerman, A. Elmali, and E. F. Wassermann, J. Magn. Magn. Mater. **238**, 11 (2002).
[11] I. Nowik, I. Felner, and E. R. Bauminger, Phys. Rev. B **55**, 3033 (1997).
[12] S.-Y. Chu, A. Cramb, M. De Graef, D. Laughlin, and M. E. McHenry, J. Appl. Phys. **87**, 5777 (2000).
[13] A. Gonzàlez-Comas, E. Obradó, Ll. Mañosa, A. Planes, V. A. Chernenko, B. J. Hattink, and A. Labarta, Phys. Rev. B **60**, 7085 (1999).
[14] E. Krén, E. Nagy, I. Nagy, L. Pál, and P. Szábo, J. Phys. Chem. Solids **29**, 101 (1968).
[15] A. Planes and Ll. Mañosa, Solid State Phys. **55**, 159 (2001).
[16] J. Marcos, Ph.D. thesis, Universitat de Barcelona, Barcelona, 2004.
[17] E. Wachtel, F. Henninger, and B. Predel, J. Magn. Magn. Mater. **38**, 305 (1983).
[18] L. Mañosa, A. Planes, M. Acet, E. Duman, and E. F. Wassermann, J. Appl. Phys. **93**, 8498 (2003).
[19] M. Wuttig, L. Liu, K. Tsuchiya, and R. D. James, J. Appl. Phys. **87**, 4707 (2000).
[20] J. Enkovaara, O. Heczko, A. Ayuela, and R. M. Nieminen, Phys. Rev. B **67**, 212405 (2003).
[21] X. Jin, M. Marioni, D. Bono, S. M. Allen, R. C. O'Handley, and T. Y. Hsu, J. Appl. Phys. **91**, 8222 (2002).
[22] M. Khan, I. Dubenko, S. Stadler, and N. Ali, J. Phys.: Condens. Matter **16**, 5259 (2004).
[23] E. Obrado, L. Mañosa, and A. Planes, Phys. Rev. B **56**, 20 (1997).
[24] T. Krenke, E. Duman, M. Acet, E. F. Wassermann, X. Moya, L. Mañosa, and A. Planes, Nat. Mater. **4**, 450 (2005).